Met. Mater. Int., Vol. 18, No. 2 (2012), pp. 265~271
doi: 10.1007/s12540-012-2009-3 Published 27 April 2012

Characterization of Deformation-Induced Metallurgical Change in Austenite Stainless Steel Sheet with Acoustic Microscopy

Yukio Kasuga[1], Tae Sung Park[2], Ik Keun Park[2,*], and Chiaki Miyasaka[3]

[1]Department of Mechanical Engineering, Tamagawa University, Tokyo, Japan
[2]Department of Mechanical Engineering, Seoul National University of Science and Technology, Seoul, Korea
[3]Department of Engineering Science and Mechanics, The Pennsylvania State University, University Park, USA

(received date: 25 March 2011 / accepted date: 18 January 2012)

This article reports on the non-destructive evaluation (NDE) of metallurgical changes induced by the deformation processes. In particular, the martensite and reversed austenite states of a meta-stable austenitic stainless steel sheet were evaluated. The sheet was elongated up to 40% at room temperature, and was then brought below room temperature to produce martensite. This was then followed by annealing for reversion. First, martensite content was measured with a Feritscope. Second, the surface acoustic wave (SAW) velocity was measured with a high numerical aperture spherically focused ultrasonic beam with a frequency equal to 600 MHz. The measured SAW velocity values were found to be dependent on the elongation, the ambient temperature during elongation, and the annealing temperature. A useful trend was found in the correlation between the measured SAW velocity and the martensite content as measured with the Feritscope. Second, using a high frequency (i.e., 800 MHz) acoustic imaging technique, the deformed and annealed grain structures were mapped. In comparing the acoustic images with the optical images, the deformed grains shown in the acoustic images were found to be significantly clearer than those shown in the optical images. These studies reveal the importance of NDE, in connection with the forming of stainless steel structures, to map the deformation induced metallurgical changes. Here, unique NDE techniques are seen to be effective in mapping the changes with the use of hypersonic SAW velocity measurements and imaging.

Key words: ultrasonics, image analysis, microstructure, tensile test, annealing

1. INTRODUCTION

Austenitic stainless steel sheets, which are usually press-formed or bent, are widely used in a variety of industrial applications ranging from pressure vessels to automobile parts, heat exchangers, electric parts and outdoor constructions [1]. This material is preferred because of its high resistance to corrosion and temperature changes. However, when the material is subjected to heating and cooling cycles, the forming accuracy, for example, in a right angle associated with a sharp bend such as a corner, is lost [2]. This phenomenon is caused by the reversion of the deformation-induced martensite to austenite when the temperature is increased. This results in the warping or misfit of a structure or an assembly, an increase in the residual stress, and the possible loss of contact members, such as trusses or beams. Therefore, significant importance must be placed on the evaluation and understanding of this process. When the martensite reverts to austenite, the timing and affected volume varies with the parameters, such as the stability of the austenite, the elongation, and the reversing temperature. Therefore, a critical need arises for the mapping of the extent of metallurgical changes on a spot by spot basis. A microprobe is required for measuring and mapping the local properties in order to achieve a map of the extent and distribution of the changes. The mechanical scanning acoustic reflection microscope (hereinafter called simply "SAM") [3] has been successfully developed into an effective microprobe. The hypersonic character is especially important because it implies a frequency range from 100 MHz to 2.0 GHz, which in turn implies not only a high resolution not available with conventional acoustic microscopes but also strong microprobe capability. Especially with the progress in the interpretation of the so-called V(z) signature [4-6], the SAM has been applied successfully for the measurement of the elastic modulus of materials [7], and for the mapping of

*Corresponding author: ikpark@seoultech.ac.kr
©KIM and Springer

residual stress [8-12] in a typically small region of about 50 micrometers in radius. However, the application of SAM to measurements on stainless steel [13] was found to be difficult because of the high absorption of hypersonic waves in the material.

In this study, in order to evaluate the appearance of the deformation-induced martensite and reversed austenite, a SAM was used that had the unique capability of measuring both phase and amplitude of the hypersonic wave reflected from the specimen [14-15]. In the experiments, typically, first, axial tension was applied to the stainless steel sheet specimen so as to produce elongation induced martensite, followed by the heat treatment to reverse the martensite to austenite. Second, the martensitic content [16] was measured with the Feritscope. Third, the SAM was used to measure and map the SAW velocities. The correlation between the SAW velocities and the degree of deformation was mapped. The measured SAW velocity values were compared and found to be in good agreement with values from the literature. Finally, the deformed and annealed grain distributions were imaged by two-dimensional scanning of the high resolution SAM probe. For the acoustic imaging, the hypersonic frequency at 800 MHz was used, with a resolution of two microns on the surface of the specimen. Furthermore, the acoustic images were compared with optical images obtained by conventional optical microscopy, with these latter represented by numerals in square brackets.

2. EXPERIMENTAL PROCEDUCES

One of the unique techniques that are central to this examination is the SAM. First, the experimental hardware of the SAM is described, whereupon the data are discussed.

2.1. Principle of Scanning Acoustic Microscopy

Figure 1 provides the schematic diagram of the apparatus constituting the scanning hypersonic microscope SAM. An electrical signal in the form of a pulse approximately 10 periods long is generated by an RF generator and sent to a piezoelectric transducer that has the form of a zinc oxide film deposited via a circulator on one end of a cylinder of single crystal sapphire. The input voltage from the transmitter to the transducer is approximately 5 V. The electrical signal is converted into a longitudinal plane elastic wave signal, which travels through the cylinder to a spherical recess referred to as the "lens." This lens is surrounded by a fluid, such as distilled bubble-free water; the lens converts the plane wave into a sharply focused beam trained on the specimen, which is also immersed in the fluid. There, the pulse is reflected and carries with it the information about the elastic properties of the specimen. Upon reaching the lens, the pulse is again converted into a plane wave by the lens and returns to the transducer through the cylinder. The elastic wave is again

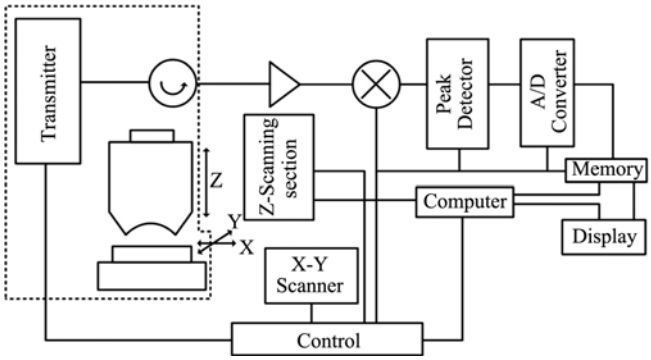

Fig. 1. Schematic diagram of SAM.

converted into an electrical signal and has a voltage of approximately 30 dB to 80 dB lower than the input voltage. After amplification, the electrical signal is selected and gated to discriminate it from unwanted signals stemming from transmission leaks and internal reflections from various uninteresting interfaces. The signal is peak-detected and stored in memory through an analog-to-digital converter. The stored signal is again converted into an analog signal by a digital-to-analog signal converter. This flow of processes allows the information that is collected at a single spot on the specimen to be displayed as intensity at a certain point on the CRT monitor. In order to form a two-dimensional acoustic image, the lens and an X-Y stage are mechanically scanned across a certain area of the specimen. The lens is able to translate axially along the z direction to vary the distance between the specimen and the lens for sub-surface focus. That is, when visualizing the surface of the specimen, the lens is focused on the specimen surface, denoted by $z = 0$ m, and when visualizing a subsurface of the specimen, the lens is mechanically defocused toward the specimen (denoted by $z = - x$ m, where x is the "defocused" distance).

2.2. Principle of Scanning Acoustic Spectroscopy

Figure 2 shows a schematic diagram of SAW propagation between the acoustic lens and the specimen via a coupling medium (e.g., distilled water). When the acoustic lens is moved toward the specimen, the voltage of the transducer changes. The plot of the changes is the so-called V(z) curve. The V(z) curve is formed by the interference at the transducer between normally reflected bulk waves and bulk waves radiated from the leaky surface acoustic waves SAW generated from bulk waves impinging onto the sample at the second critical angle of refraction.

Figure 3 shows an example of the V(z) curve. The specimen is silica glass. The temperature of the coupling medium (i.e., de-ionized water) is 23. The operating frequency of the acoustic lens (Olympus; model: AL4M631) is 400 MHz. The velocity of the SAW is expressed as Eq. (1) from the spacing of the minima Dz in Fig. 3.

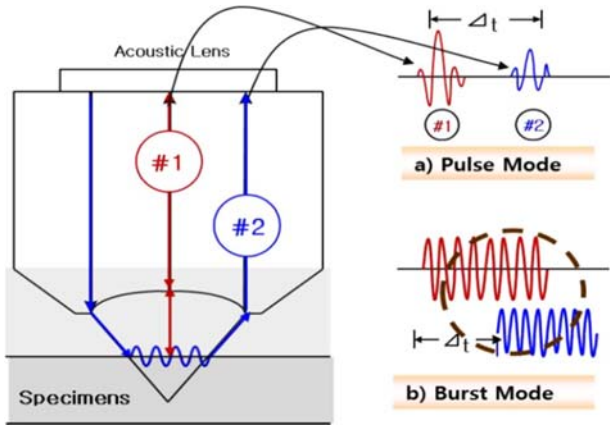

Fig. 2. Schematic diagram showing the principle of the V(z) curve.

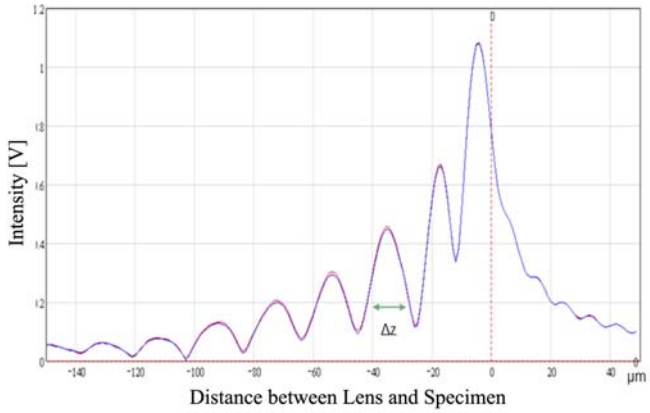

Fig. 3. Example of the V(z) curve.

$$V_{saw} = \frac{V_w}{\sqrt{1-\left(1-\frac{1}{2}\cdot\frac{V_w}{\Delta z\cdot f}\right)^2}} \tag{1}$$

where V_{saw} is the velocity of a surface acoustic wave propagating on the specimen, V_W is the velocity of the longitudinal wave of the coupling medium, and f is the frequency of the ultrasonic wave emitted from the acoustic lens [17].

$$V(z) = C^{-1}\int_0^{\infty} u^2(r)P^2\left(\frac{r}{f}\right)\exp\left\{i2kz\sqrt{1-\left(\frac{r}{f}\right)^2}\right\}rdr \tag{2}$$

where u is an acoustic field, P is a pupil function, R is a reflectance function, k is a wavelength in the coupling medium, f is a focal length and C is expressed as the following equation;

$$C = \int_0^{\infty} u^2(r)P^2(r)rdr \tag{3}$$

Equations (2) and (3) are expressed by using $r = f\sin\theta$, as follows:

$$V(z) = C\int_0^{\infty} u^2(\theta)P^2(\theta)R(\theta)\exp(i2kz\cos\theta)\sin\theta\cos\theta d\theta \tag{4}$$

$$C = \int_0^{\theta_o} u(\theta)\sin(\theta)\cos\theta d\theta \tag{5}$$

where θ is half the aperture angle of a lens.

When using $k_z = k\cos\theta$, Eqs. (4) and (5) are expressed as follows:

$$V(z) = C^{-1}\int_k^{k\cos\theta_o} Q^2(k_z)R(k_z)\exp(i2kz)dk_z \tag{6}$$

$$C = \int_k^{k\cos\theta_o} Q^2(k)dk_z \tag{7}$$

$$Q^2(k_2) = u^2(k_z)P^2(k_z)k_z \tag{8}$$

From Eq. (6), the following equation is obtained.

$$\mathcal{F}^{-1}\{V(z)\} = C^{-1}Q^2(k_z)R(k_z) \tag{9}$$

where $\mathcal{F}^{-1}\{\}$ is the inverse Fourier transform. Liang *et al.* showed that the reflectance function of the specimen can be calculated by the Inverse Fourier Transform of the complex V(z) curve (including amplitude and phase), so that the longitudinal, shear and Rayleigh wave velocity of the material itself can be directly obtained [18]. In this study, we used a SAM including capabilities (Olympus; model: EPA02) to analyze the phase transformation of the metastable austenitic stainless steel.

2.3. Specimen Description

Table 1 shows the chemical composition of the materials. The deformation-induced matensite was produced by applying axial tension to strip sheet samples typically having dimensions of: thickness 1.0 mm, width 10 mm and length 120 mm. The ram speed was 4.58 mm/s and the range in elongation was from 5% to 40%. The ambient temperature T_f was assigned to be 83 K, 203 K, 273 K and 293 K by dipping samples into liquid nitrogen, dry ice, ice water, and running water, respectively. The temperatures were measured with a precision of ±1.0 K. The elongated specimens were annealed in vacuum. Figure 4 shows the heating and cooling rates of the specimens. Heating and cooling rates were 5.6 K/min and 1.4 K/min, respectively. The annealing time was 30 min. Annealing temperatures T_a were chosen to be 623, 823, 1023 and 1223 K. Specimens were cut carefully into 3 pieces with a high-speed disk cutter during wet conditions. The specimen surfaces were ground with carborundum paper of successively finer grades down to #1200. This was followed by polishing successively with 1.0 μm and 0.25 μm

Table 1. Chemical composition of material (mass %)

C	Si	Mn	P	S	Ni	Cr	Mo	N
0.070	0.71	1.04	0.027	0.004	7.09	16.99	0.19	0.027

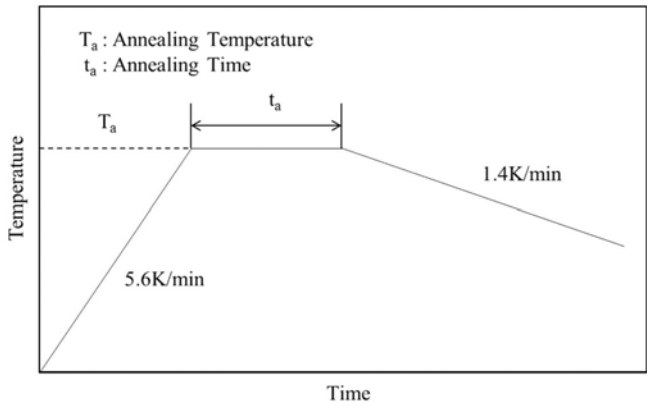

Fig. 4. The heating and cooling rate of the specimens.

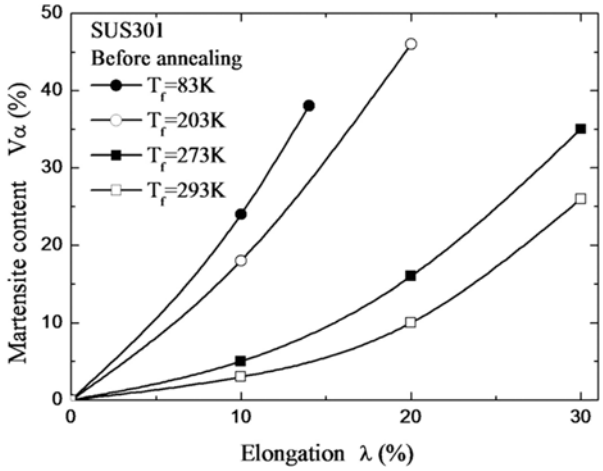

Fig. 5. Effect of elongation on martensite content.

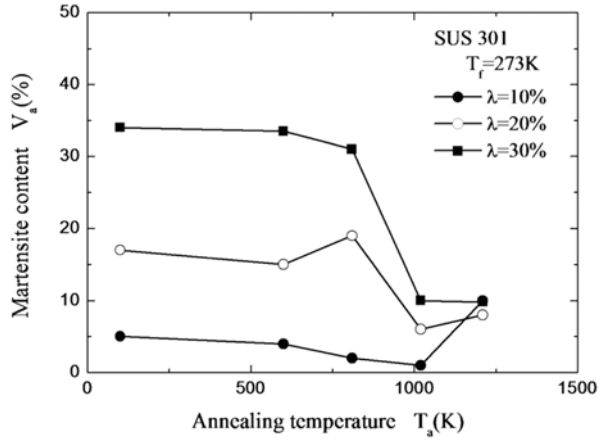

Fig. 6. Change in martensite content (T_f = 273 K).

diamond paste for the final stage. The specimens were then etched for about 10-15 minutes by dipping them into a combined solution of 20 ml ethanol, 80 ml hydrochloric acid and 1.0 g picric acid.

2.4. Acoustic image Acquisition

The change in the grain microstructures was observed by imaging the specimens with the SAM (Olympus; model: UH3) at a frequency of 800 MHz. This high frequency was chosen on the basis of the need to resolve the grain structure.

A Feritscope (Fisher Co., Ltd.) was used to measure the content values of both deformation-induced martensite caused by axial tension and the remaining martensite after incomplete reversion. The values were then adjusted by taking the thickness into consideration.

3. EXPTAL RESULTS

3.1. Martensite Content

Figure 5 shows the relationship between the degree of elongation and the martensite content when the temperature was changed. As the elongation is increased, the martensite content is also increased proportionally. The lower the temperature, the larger is the increase in martensite content, with the elongation unchanged. This shows that the martensite content is dependent on both the temperature during elongation and the degree of elongation itself.

Figure 6 shows the change in martensite content when the sheet was elongated at T_f = 273 K and then annealed. The values at T_a = 273 K are the values when the sheet is not annealed. When the annealing temperature was gradually increased, the content of martensite was decreased. Furthermore, the content became almost zero at T_a = 1223 K. This means that the deformation-induced martensite is completely reversed back to austenite. In SUS301 stainless steel, a similar phenomenon can be seen. However, at T_a = 1223 K, the martensite is not completely decreased, and content of about 5~10 % remains. This is explained by the reversal of the change in the material, which has been reversed to austenite in the process of heating, and to martensite in the process of cooling. Takagi *et al*. have pointed out this phenomenon [19]. Starting and finishing temperatures for reversion are considerably higher than those obtained by Takagi *et al.* [20]. This is due to the low stability in austenite and the insufficient plastic deformation (elongation is at most 40% in the state of axial tension).

Figure 7 shows the remaining martensite content when the specimen was annealed after the elongation (10%). The martensite content decreased as the annealing temperature was increased. When the temperature was more than 1023 K, almost no martensite remained. This observation suggests that the deformation-induced martensite is almost completely changed to austenite. The remaining martensite content was found to decrease with the increase in the annealing temperature. Martensite content was significantly increased with the temperature at 1223 K. These results match the results shown in Fig. 6.

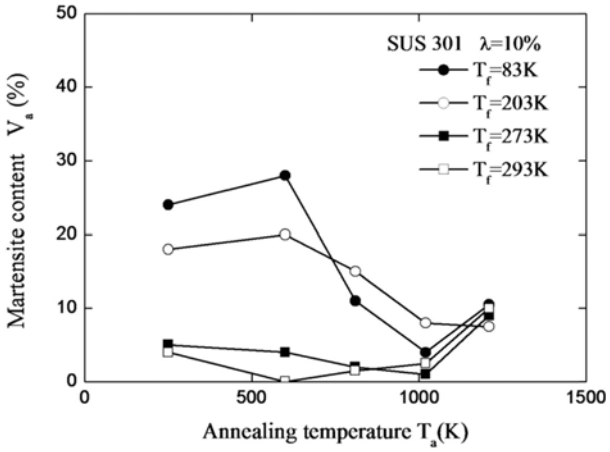

Fig. 7. Martensite content after annealing (λ = 10 %).

3.2. SAW Velocity Measurement

Figure 8 shows the change in SAW velocity due to the elongation. The error in the velocity value obtained in the experiment is at most ±50 m/s and the relative error is 3.6% under the assumption that the velocity is 2800 m/s. This error became smaller as the martensite content increased. The velocity increased as the elongation increased for either of the materials. The lower the ambient temperature was, the higher the velocity became with the same elongation. At temperatures T_f = 83 K and 293 K, no monotonic increase in velocity could be observed. When T_f was 293 K, the martensite content was found to be below 10%, regardless of the elongation up to 30%. This is seen to lead to the small change in velocity. From the readings of the Feritscope, it can be seen that when T_f is 83 K, consideration of and compensation for the thickness is not enough to obtain true martensite content. Actually, more martensite than is shown in the result in Fig. 8 is thought to appear. If this were accurately estimated, martensite would be seen to accumulate sufficiently, even with the lower elongation.

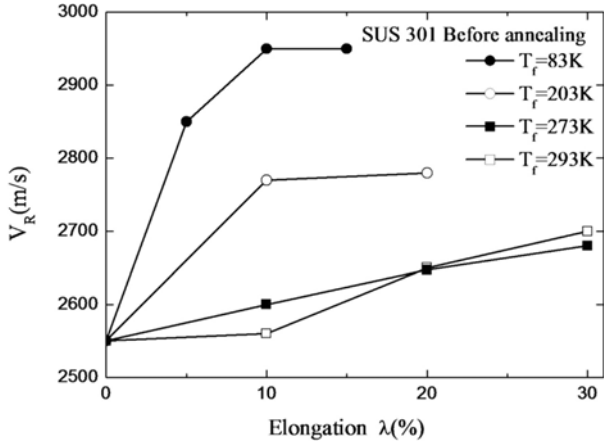

Fig. 8. Effect of elongation on Rayleigh wave velocity.

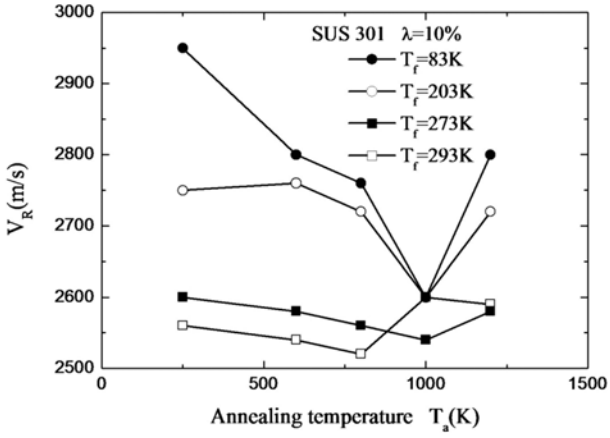

Fig. 9. Effect of annealing temperature on SAW velocity.

Figure 9 shows the relationships between the elongation and the SAW velocity in SUS301 after annealing. An annealing temperature of T_a = 273 K means that the heat treatment is not performed. As the temperature T_a increases, the velocity decreases and achieves a minimum at 1023 K. When the temperature increases the SAW velocity increases. This result is similar to the result shown in Fig. 7.

3.3. Microstructures of Specimens

Figure 10 provides acoustic and optical images of the specimens before annealing. The configuration of the grain

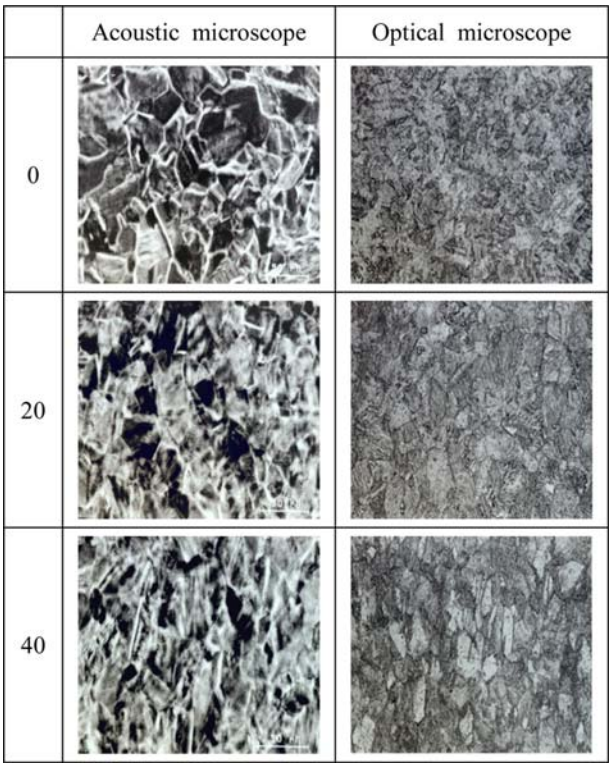

Fig. 10. Acoustic and optical images (before annealing), Frequency: 800 MHz, Defocusing Distance: –4 μm.

can clearly be seen in the case of no elongation: an M_s point exists in the range of the room temperature when the martensite is in the process of cooling. This means that there is a trace of martensite even when the elongation is zero. In this experiment, the change in the SAW velocity was larger than that in the density due to the deformation-induced transformation and reversion. This observation suggests that the acoustic impedance depends strongly on the change in velocity. This fact is also corroborated by the measurements the Feritscope. The average grain size could be estimated to be in the range of 30 μm to 50 μm. As the sheet was elongated, the grains aligned themselves in the longitudinal direction and the increase in martensite could clearly be seen in the grains.

For comparison, optical images were obtained with a conventional optical microscope (Olympus, model: BH2). It is necessary to etch the surface of the specimen in order to observe the grain boundaries of the induced martensite, so that the changes in the direction of the grain boundary and the grain size can be observed by optical microscopy. Therefore, the deformation-induced martensite in the optical images can be compared with that in the acoustic images. The SAM appeared to give better images than the optical microscope when used for observation of the grain structure.

The grain structures after annealing are shown in Fig. 11. When the specimen was annealed at 823 K, the structure was found to be approximately the same as that before annealing;

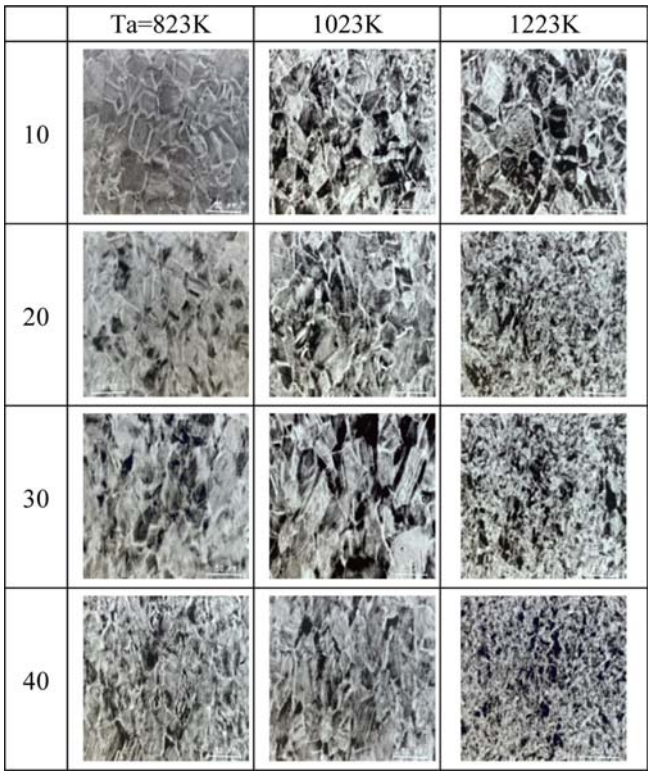

Fig. 11. Acoustic image (after annealing), Frequency: 800 MHz, Defocusing distance: –4 μm.

martensite, which can be seen as white stripes, decreased as the temperature was raised to 1023 K, especially in the cases of 20% and 30% elongation. Furthermore, at 1223 K, the martensite content was found to be greatly increased for all elongations with the exception of the elongation of 10%. Despite the magnification of the field of view, it was difficult to observe the grain clearly. When used for observation of the grain structure, the SAM appeared to give better images than those of the optical microscope.

4. DISCUSSION

In the experiments, an acoustic lens was used with a measuring area of about 190 μm. Based on the images of the observed grain structures, there are many small grains within this area. Therefore, the material was assumed to be approximately isotropic. The longitudinal and shear wave velocities can be expressed as follows:

$$V_L = \sqrt{\frac{(1-\nu)E}{(1+\nu)(1-2\nu)\rho}} \tag{12}$$

$$V_T = \sqrt{\frac{E}{2(1+\nu)\rho}} \tag{13}$$

where V_L is the velocity of the longitudinal wave, V_T the velocity of the transverse wave, E Young's modulus, ν Poisson's ratio, and ñ density, and the relationship among V_R, V_L and V_T is expressed as follows:

$$\left(\frac{V_R}{V_T}\right)^6 - 8\left(\frac{V_R}{V_T}\right)^4 + V_R^2\left(\frac{24}{V_t^2} - \frac{16}{V_l^2}\right) - 16\left\{1 - \left(\frac{V_T}{V_L}\right)^2\right\} = 0 \tag{14}$$

Equation (14) can be transformed using Eqs. (12) and (13) when Poisson's ratio is given, and V_R can be obtained. For example, when ν is 0.3, $V_R = 0.927V_T$. This means that the value for the SAW velocity can be obtained when Young's modulus and density are known, in addition to Poisson's ratio. The strip sheets after elongation and annealing were used to obtain Young's modulus and Poisson's ratio. On the surface of the strip sheet, a two-axis rosette strain gauge was adhesive-bonded and the strip was elongated within the elastic range. The density of the material was measured with a densitometer (model; JIS-Z8807).

5. CONCLUSIONS

Deformation-induced transformation and reversion processes of stainless steel were evaluated with a Feritscope, a hypersonic microscope and an acoustic spectrometer. Stainless steel SUS301 strip sheets of 1.0 mm thickness were elongated and then annealed. The martensite content was measured after elongation by axial tension and annealing; the effects of elongation, ambient temperature and annealing

temperature were examined. Afterwards, the SAW velocity values were obtained by the complex V(z) method under a variety of conditions. The surface of the material was imaged by scanning acoustic microscopy and conventional optical microscopy. The following important conclusions were ascertained.

(1) The lower the ambient temperature, the larger the elongation and the lower the stability of the material, the more martensite appeared. After annealing, the martensite content decreased as the deformation-induced martensite underwent a reversion process. For unstable SUS301, the martensite content increased again when annealed at the higher temperature.

(2) The SAW velocity increased with increasing elongation or decreasing temperature.

(3) Furthermore, it is possible to estimate the extent of the transformation process for stainless steel with SAM, if the SAW velocity changes due to the deformation-induced martensite were separated from the changes due to the reversion process.

ACKNOWLEGMENTS

This work was supported by a National Research Foundation of Korea (NRF) grant funded by the Korean government (MEST) (No. 2011-0019195) (No. 2011-0017970) (No. 2011-220-D00002), and Seoultech. The authors would like to thank Mr. Tomio Endo (Olympus) for his help with acoustic spectroscopy.

REFERENCES

1. S. M. Hong, J. J. Park, M. K. Lee, and C. K. Rhee, *Korean J. Met. Mater.* **48**, 893 (2010).
2. Y. Kasuga, *J. Mater. Processing Technol.* **60**, 233, (1996).
3. A. Atalar, C. F. Quate, and H. K. Wickramasinge, *Appl. Phys. Lett.* **31**, 791 (1977).
4. R. D., Weglein, *Appl. Phys. Lett*. **34**, 179 (1979).
5. W. Parmon and H. L. Bertoni, *Electron. Lett.* **15**, 684 (1979).
6. A. Atalar, *Appl. Phys.* **49**, 5130 (1978).
7. J. Kushibiki, T. Ueda, and N. Chubachi, *Ultrasonics Symp. Proc., IEEE*, p. 817, New York (1987).
8. M. Obata, H. Shimada, and T. Mihara, *Exp. Mech*. **30**, 34 (1990).
9. C. Miyasaka and B. R. Tittmann, *ASME* **127**, 214 (2005).
10. C. Miyasaka, B. R. Tittmann, and S. Tanaka, *ASME* **124**, 336 (2002).
11. E. Drescher-Krasicka, *J. Acoust. Soc. Am*. **94**, 453 (1993).
12. E. Drescher-Krasicka and J. R. Willis, *J. Nature* **384**, 52 (1996).
13. Ph. Dombret, *Nuclear Eng. Design* **131**, 279 (1991).
14. T. Endo, Y. Sasaki, T. Yamagishi, and M. Sakai, *Jpn. J Appl. Phys.* **31**, 160 (1992).
15. Y. Sasaki, T. Endo, and T. Yamagishi, *IEEE Transaction on Ultrasonics*, **39**, 638 (1992).
16. H. C. Fiedler, B. L. Averbach, and M. Cohen, *ASM* **47**, 26 (1955).
17. A. Atalar, *Appl. Phys* **50**, 8237 (1979).
18. K. K. Liang, G. S. Kino, and B. T. Khuri-Yakub, *IEEE Trans. Sonics Ultrason*. **32**, 213 (1985).
19. S. Takagi, S. Tanimoto, K. Tomimura, and Y. Tokunaga, *Tetsu to hagane* **74**, 1052 (1988).
20. S. Takagi, S. Tanimoto, K. Tomimura, and Y. Tokunaga, *Tetsu to hagane* **74**, l058 (1988).